

Development of multiferroic polymer nanocomposite from PVDF and $(\text{Bi}_{0.5}\text{Ba}_{0.25}\text{Sr}_{0.25})(\text{Fe}_{0.5}\text{Ti}_{0.5})\text{O}_3$

C. Behera^{1,2} · R. N. P. Choudhary¹ · P. R. Das³

Received: 1 June 2016 / Accepted: 5 October 2016 / Published online: 13 October 2016
© Springer Science+Business Media New York 2016

Abstract Thin films of some polymer–ceramics multiferroic nanocomposites (in 0–3 connectivity) of compositions $(1-x)\text{PVDF}-x((\text{Bi}_{0.5}\text{Ba}_{0.25}\text{Sr}_{0.25})(\text{Fe}_{0.5}\text{Ti}_{0.5})\text{O}_3)$ ($x = 0., 0.50, 1, 0.15$) have been prepared using a standard solution casting method. The basic structure and surface morphology of the materials were studied using X-ray diffraction and scanning electron microscopy technique respectively. Structural investigation confirms the presence of polymeric electro active β -phase of matrix (PVDF) and nano filler perovskite phase of the incorporated nano-ceramics. The high resolution transmission electron micrograph of the prepared nano-ceramic thin film composite has shown distinct and uniformly distributed particles (with less agglomeration). This has been observed in SEM micrographs also. The flexible nano-composites fabricated with polymer (PVDF), bismuth ferrite (BiFeO_3) and ferroelectric (BST) exhibit high dielectric constant and low tangent loss. The electric response investigated by impedance spectroscopy technique in terms of electric circuit has provided some interesting results on contributions of grain and grain boundary in the restive characteristics of the composites. The study of ac conductivity as a function of frequency obeys Jonscher's power law. The experimentally

obtained first order magnetoelectric coefficient (α_{ME}) is found to encouraging for multifunctional application. The improved conductivity and dielectric properties suggest some promising applications in the embedded capacitors.

1 Introduction

Multiferroic materials with high magneto-electric (ME) coupling coefficient have attracted much attention of scientists and technologists because of some potential applications of the materials in different emerging technological fields such as spintronics, sensor fabrication, magnetic storage, novel circuits and high power applications. The design and development of such type of materials with strong magneto electric coupling between magnetic and electric polarizations are very much required for the above applications. It is a very rare phenomena where magnetic ordering (associated with unpaired or partly filled d or f electron) and ferroelectric ordering (where an empty outer shell ' d ' electron) exist in a single phase of the materials. Many attempts have been made to overcome the difficulty to fabricate hybrid multiferroic composite materials of diverged properties. Some composite structures of ferrite–piezoelectric ceramics, ferrite–lead zirconate–titanate, ferrite–lead iron niobates, etc., have been found to exhibit much higher ME coupling coefficient as compared to that of mono-phase multiferroics. As PVDF has many interesting properties and advantages over other polymers, it has been selected to fabricate inorganic–organic nanocomposites in PVDF matrix with expectation to provide excellent dielectric and required properties as compared to traditional multilayer ceramics, polymer-based multiferroic composites in the thin film form offers several advantages such as easy and cost effective processing, mechanical flexibility, light weight and the ability to form any desired shape and size of samples required for devices.

✉ C. Behera
cdbehera1986@gmail.com

¹ Multifunctional and Advanced Materials Research Laboratory, Department of Physics, Institute of Technical Education and Research, SOA University, Bhubaneswar 751030, India

² Present Address: Department of Physics, NIT Agartala, Tripura, India

³ Department of Physics, V S S University of Technology, Burla, Sambalpur, Odisha, India

After the discovery of piezoelectricity in polyvinylidene fluoride (PVDF), the interest has been generated for its piezoelectric and pyroelectric application [1, 2]. There are three different type of relaxation process in the, β and γ phases of the material. The relaxation processes appear from high temperature to the low temperature side and from low frequency to high frequency side. The primary relaxation process is attributed to the rotation of dipoles from one quasi-stable state to another in which the diffusion motion of the segment occurs. The β relaxation is associated with the partial orientation of the dipoles in the range of local environments where the large scale arrangement of the main chain is frozen. Earlier the molecular vibration of the α , β and γ phases of PVDF have been investigated [3]. The distribution of relaxation times from dielectric spectroscopy, using Monte Carlo simulation, in α -PVDF reveals two relaxation process i.e., α_a —relaxation process associated with glass transition and α_c —relaxation process due to changes in confirmation in the crystalline region [4]. As it is well known that PVDF possesses low acoustic impedance having excellent matching with water and human tissue, making this polymer very useful for underwater acoustics and medical imaging application. All these fascinating properties of PVDF can be used for device application. It is very important to mention that the different form and film processing methods of PVDF material are very important. As many technique such as injection modeling, die-casting, solution casting, solution evaporation technique hot rolling etc., solution casting is one of the desired and economical method for preparing desired thickness thick as well as thin film. In order to increase the dielectric constant of a polymer the strategy is to follow by increasing the incorporation of perovskite ceramic filler (such as BaTiO_3 , $\text{Ba}_x\text{Sr}_{1-x}\text{TiO}_3$, $\text{Pb}(\text{Zr},\text{Ti})\text{O}_3$) with high dielectric constant into the polymer matrix [5–7]. But the ability of spherical ceramic particles to increase the dielectric constant is very weak at low volume fraction based on Maxwell-Garnett model rule of mixture [8]. Higher loading of the ceramic fillers is usually needed to realize a high dielectric constant, and in such a case the, composite exhibit deteriorated break down strength, mechanical and processing properties. That is why we have prepared the ceramic polymer nano-composite $(1-x)\text{PVDF}-x((\text{Bi}_{0.5}\text{Ba}_{0.25}\text{Sr}_{0.25})(\text{Fe}_{0.5}\text{Ti}_{0.5})\text{O}_3$ ($x = 0.05, 0.1, 0.15$)) still we have achieved encouraging dielectric properties and multiferroic properties for suitable device application.

2 Experimental

The complex nono-ceramics of $(\text{Bi}_{0.5}\text{Ba}_{0.25}\text{Sr}_{0.25})(\text{Fe}_{0.5}\text{Ti}_{0.5})\text{O}_3$ (BFO–BST) multiferroic was fabricated by mechanical alloying method followed by thermal treatment and has been reported by us in our previous report [9]. The synthesis started with the ball milling of required

proportion of high-purity ingredients (>99.9 %): Bi_2O_3 , BaCO_3 , SrCO_3 , Fe_2O_3 , and TiO_2 (from M/S Loba Chemicals Co. In) along with 4 % extra Bi_2O_3 in order to avoid the bismuth loss during high-temperature processing. Above raw materials were milled in a high-energy ball mill (M/s Retsch-Planetary Ball Mill, Model PM 100, Germany) in the toluene media with different milling parameters (i.e., milling speed = 450 rpm; milling time: 90 h ball to mass ratio 10:1; diameter of ball 10 mm in zirconium vial of 125 ml capacity). After 90 h of milling the milled powders were calcined at an optimized temperature 1000 °C for 4 h to form the desired phase of the compound. Then the prepared powder was subsequently thoroughly mixed with a small amount of binder material (polyvinyl alcohol) and compacted into disks (10 mm in diameter, 1 mm thickness) at an iso-static-pressure of $5 \times 10^8 \text{ kg/m}^2$. The discs (pellets) were sintered at 1050 °C for 4 h. That ceramic powder sample was taken without any further purification for the synthesis of ceramics polymer nanocomposites. The composites of the composition $(1-x)\text{PVDF}-x(\text{Bi}_{0.5}\text{Ba}_{0.25}\text{Sr}_{0.25})(\text{Fe}_{0.5}\text{Ti}_{0.5})\text{O}_3$ ($x = 0.05, 0.1$ and 0.15) were fabricated by a solution-casting method. For the fabrication of composites, NMP-(*N*-Methyl-2-Pyrrolidone) was used as a solvent for PVDF. The solution for the composite was prepared at 60–70 °C under constant stirring with the help of a magnetic stirrer until the complete dissolution of the polymer and ceramic was obtained. The homogenous suspension was then poured on the glass substrate of laboratory-fabricated micrometer-controlled tape caster, and then allowed to dry in air for few days to remove solvent traces. The thin film was then peeled off from the glass substrate. Phase analysis of the fired samples as well as the prepared polymer thin films were carried out using diffraction data collected by an X-ray powder diffractometer at a scanning rate of 3°/min in the range of $20^\circ < 2\theta < 80^\circ$ using $\text{CuK}\alpha$ radiation. The surface morphology of the sintered pellets and fabricated ceramic–polymer composite thin film samples were investigated by scanning electron microscopy (ZEISS-SEM). The ferroelectric and magnetic properties of the ceramic–polymer nanocomposite were carried out by P–E loop tracer (M/S-Radiant Technology, USA) and SQUID (EverCool SQUID VSM DC magnetometer Quantum Design, USA) respectively. Then the pellet samples were polished and electrode with high purity silver-paste for electrical the measurements of electrical parameters such as capacitance, impedance, tangent loss and other dielectric parameters using computer-controlled phase sensitive meter (LCR/impedance analyzer) (M/S N4L model PSM 1735, UK) in a wide frequency range (1 kHz–1 MHz) different temperatures (25–125 °C). All the above electrical parameters of the ceramic–polymer composite have been measured with the pre-mentioned

instrument. Magneto-electric measurement was performed by a ME set up (Marine India) connected to a lock in amplifier. In this experiment, the DC magnetic field up to 7 kOe was produced by an electromagnet whereas AC magnetic field was produced by a Helmholtz coil having 200 turns with a radius of 2.5 cm. For the magneto-electric measurement of the ceramic–polymer composite were placed in the magnetic field with its faces perpendicular to the field direction. The ME voltage developed across the sample was measured using a Lock in Amplifier (SR830).

3 Results and discussion

3.1 Structural and micro-structural analysis

The room temperature XRD pattern along with its refined parameters of $(\text{Bi}_{0.5}\text{Ba}_{0.25}\text{Sr}_{0.25})(\text{Fe}_{0.5}\text{Ti}_{0.5})\text{O}_3$ indicate that it crystallizes in Rhombohedrally distorted crystal system with R3c space group having lattice parameters: $a = 5.6115$ and $c = 13.7357 \text{ \AA}$ which is consistent with the reported ones [10] as well as with our previous report [9].

Figure 1 compares the X-ray diffraction patterns of PVDF and BFO–BST and $(1-x)\text{PVDF}-x(\text{Bi}_{0.5}\text{Ba}_{0.25}\text{Sr}_{0.25})(\text{Fe}_{0.5}\text{Ti}_{0.5})\text{O}_3$ ($x = 0.05, 0.1$ and 0.15) ceramic–polymer nano-composite. The pure PVDF spectra show the presence of both crystalline and amorphous phases of PVDF. The pattern also shows that the PVDF exists in mixed α - and γ -phase. The most prominent peak of the material appears for all the phases around 20° but for α - and γ -phase a second peak appears around 18° which makes them easy to distinguish from the β -phase. There are two intense peaks appearing at diffractions angle 2θ corresponding to 20° and 39.3° assigning to $\beta(110)$ plane and $\alpha(002)$ plane [11, 12]. The peaks at 2θ corresponding to 18.4° (020) and 36.2° (200) could be indexed to the α - and γ -phase of PVDF respectively [13]. The XRD patterns of

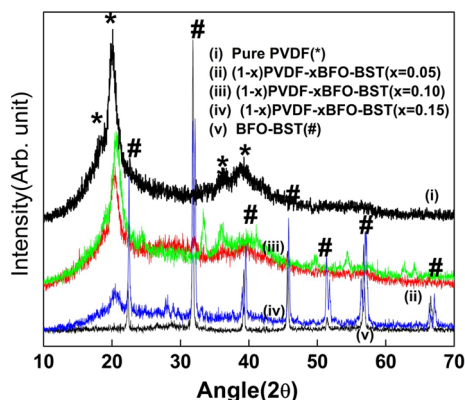


Fig. 1 Represents the XRD of (i) pure PVDF, (v) BFO–BST ceramics and $(1-x)\text{PVDF}-x$ BFO–BST with (ii) $x = 0.05$, (iii) $x = 0.10$ and (iv) $x = 0.15$ of the polymer nanocomposite

$(1-x)\text{PVDF}-x(\text{Bi}_{0.5}\text{Ba}_{0.25}\text{Sr}_{0.25})(\text{Fe}_{0.5}\text{Ti}_{0.5})\text{O}_3$ ($x = 0.05, 0.1$ and 0.15) composite with different volume fraction of BFO–BST fillers. It shows the presence of both PVDF and BFO–BST phases (as marked by # and *). Due to low level of filler concentration ($x = 0.05$ and 0.10), strong diffraction peak of PVDF is found to be dominate. But in case of $x = 0.15$ of ceramic filler the perovskite phase seems to dominate which is due to the strong diffraction of the incorporated ceramic. This confirms that the proper incorporation of the ceramic powder into the PVDF matrix. This type of observation was reported by others also [14].

The SEM micrograph of BFO–BST and PVDF nano-composite are shown in Fig. 2 and shows that the BFO–BST particles are well dispersed in the PVDF polymer matrix with negligibly small agglomeration of fine ceramic particle. The HRTEM micrograph of the BFO–BST ceramics reveals the nanonature of the particle with less agglomeration. More pores are observed in the composite which may be due to the contraction of PVDF during the solidification process [15].

3.2 Dielectric properties

Figure 3 Shows the variation of relative dielectric constant (ϵ_r) and tangent loss ($\tan \delta$) with frequency of BFO–BST, PVDF and $(1-x)\text{PVDF}-x(\text{Bi}_{0.5}\text{Ba}_{0.25}\text{Sr}_{0.25})(\text{Fe}_{0.5}\text{Ti}_{0.5})\text{O}_3$ ($x = 0.05, 0.1, 0.15$) composite at room temperature. The values of dielectric constant and loss of pure PVDF has already been published by one of the authors in the previous report [16]. The values of dielectric constant of PVDF is 7–13 as reported by other [17, 18], and loss value is also very small. Here we have also same agreement with the previously reported dielectric value and it is found to be within 10. The value of dielectric constant of different filler concentration loaded ceramic–polymer nano-composite is comparably high than that of pure PVDF and lower than that of BFO–BST ceramic. The inset of Fig. 3 provides the dielectric data of BFO–BST nano-ceramic. When the filler (ceramics) concentration of composites increases from 5 to 15 %, then the dielectric constant decreases. From X-ray data it has been confirmed that α - and γ -phases are present in PVDF (which are both non-polar). Because of the non-polar nature of PVDF and the constrained polymer chain which obstructs the formation of electrical polarization, the value of dielectric constant of $(1-x)\text{PVDF}-x(\text{Bi}_{0.5}\text{Ba}_{0.25}\text{Sr}_{0.25})(\text{Fe}_{0.5}\text{Ti}_{0.5})\text{O}_3$ ($x = 0.05, 0.1, 0.15$) is less than the that of BFO–BST ceramics [19] where as the opposite trend is observed in case of $\tan \delta$ spectrum. The decreasing its value on increasing frequency can be attributed to the fact that the motion and rotation of dipoles in the PVDF phase cannot keep up with the change in the frequency of the electrical field. In other words, at higher frequency, the

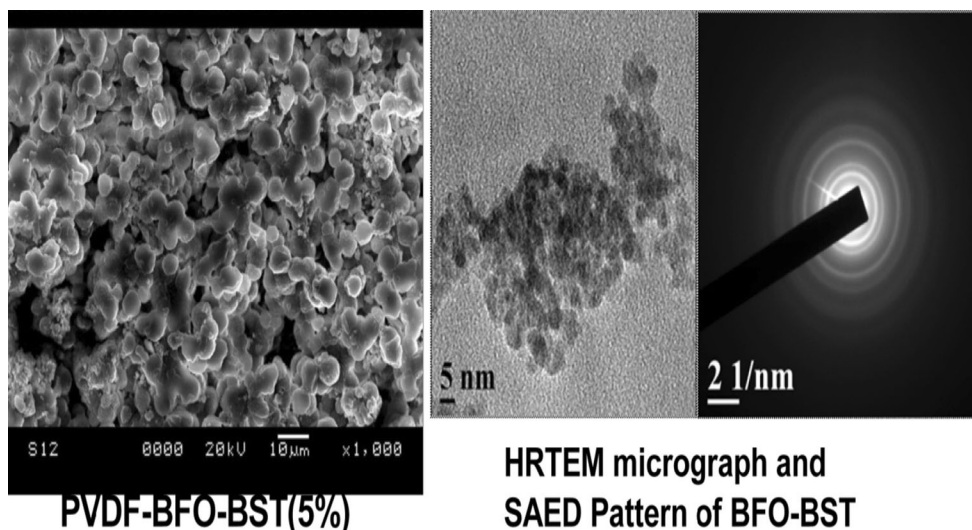
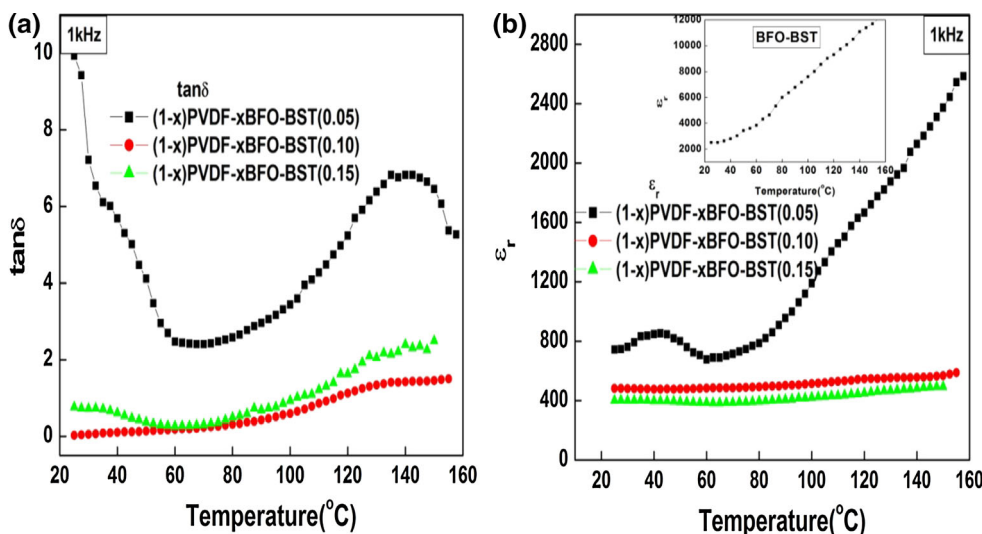


Fig. 2 SEM Micrograph PVDF–BFO–BST (5 %) and HRTEM micrograph along with SAED pattern of BFO–BST nanoceramics

Fig. 3 Temperature dependent tangent loss (a) and dielectric constant (b) of (1 – x)PVDF–xBFO–BST (x = 0.05,0.10,0.15) nanocomposite compared at 1 kHz



electric field changes with faster rate. It sustains the polarization effect resulting in the reduction of the dielectric constant [20]. The dielectric constant increases with rise in temperature for (1 – x)PVDF–x((Bi_{0.5}Ba_{0.25}Sr_{0.25})(Fe_{0.5}Ti_{0.5})O₃) (x = 0.05,0.1,0.15)) which suggests that due to conductive increase of BFO–BST and thermal expansion of PVDF with increasing temperature. At low frequency, the molecules have enough time to polarize. But in case of high frequency, the polarization of molecules does not have enough time to catch up with the change in electrical field frequency, which leads to the weak dependence of dielectric constant on temperature [21].

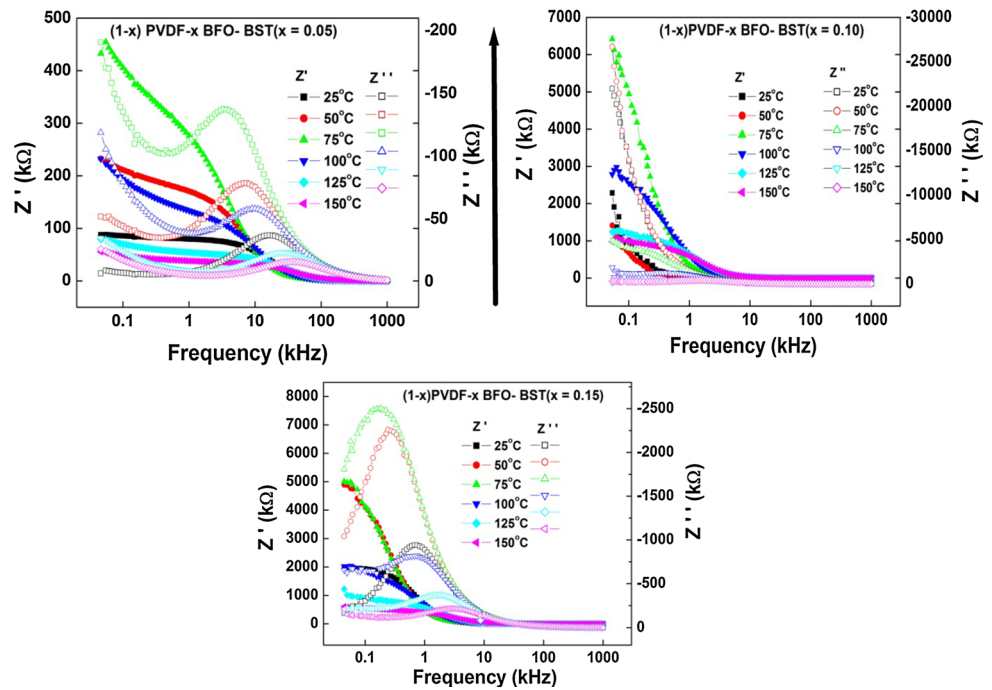
3.3 Impedance spectroscopy

The origin of dielectric relaxation mechanism associated with dynamics of bound or mobile charges in the bulk or interfacial

regions of the studied materials could be understood by using the complex impedance spectroscopy (CIS) technique.

The variation of both real (Z') and imaginary part of impedance (Z'') with frequency from 25 °C temperature to 150 °C with an interval of 25 °C of (1 – x) PVDF–x(BFO–BST) (x = 0.05,0.10,0.15) presented in Fig. 4. It has clearly been observed that Z' has higher value at lower frequencies and it decreases monotonically with rise in frequency and attain a constant value at higher frequencies at most of the temperatures. This trend (attainment of constancy of Z' value) appears to be shifting gradually towards the high frequency side with rise in temperature, and its value for all temperatures merge in the high frequency domain. The decrement in the real part of impedance (Z') with the rise in temperature and frequency may be due to the increase in ac conductivity with rise in temperature and frequency. The merger of the real part of

Fig. 4 Frequency dependent Z' and Z'' spectrum of $(1-x)$ PVDF- x (BFO-BST) ($x = 0.05, 0.10, 0.15$)



impedance (Z') for all temperatures in the high frequency domain indicates a possibility of the release of space charge as a result of lowering in the barrier properties of the composite. This dispersion region spreads to a higher frequency with increase in temperature.

From the frequency dependence of the imaginary part plot of impedance (Z'') of $(1-x)$ PVDF- x (BFO-BST) ($x = 0.05, 0.10, 0.15$) a characteristic frequency ($\omega_{\max} = 2 - \pi f_{\max}$) peak appears which depends on temperature as well as filler concentration. The appearance of double relaxation in $x = 0.05$ composite suggests the relaxation process is quite dependent on temperature as well as filler concentration. This peak can be related to the type and strength of the electrical relaxation phenomena in the material. Peaks are more prominent at higher temperature and progressively become more obvious as the temperature increases and the concentration of filler. With the increase in filler concentration the resistance of the composite increases because of the high resistive BFO-BST nanoparticles. For that reason the resistance decreases with increase in filler concentration. This is a clear indication of stronger relaxation at higher temperature. It can be seen that the curves display broad and symmetric peak. Relaxation occurs over several frequency decades. This symmetric shape of the peaks can be assigned to the multiple relaxation and deviation from Debye behavior. As the temperature increases, the maximum of Z'' shifts to higher frequency. At higher frequency, the space charge has less time to relax and the recombination would be faster. At higher frequency, the space charge polarization reduced so the curves merge there.

Figure 5 shows the Nyquist plots between $Z'(f)$ and $Z''(f)$ for ceramics and ceramic polymer nano-composite from room temperature to 150 °C. The impedance spectrum comprising of one or more semicircles distinguishes the contributions of grains (g) and grain boundary (g_b) in the resistive characteristics of the materials. The two semicircles in the figure represent two types of relaxation processes occurring in the material that corresponds to grain (in the high-frequency range) and grain boundary (in the low-frequency range). The electrical properties of the sample could be represented by an equivalent circuit comprising of parallel combination of two RC and RCQ circuits. Where Q being the constant phase element. The different configuration of ceramic-polymer nano-composite shows decrease of slope on increasing temperature. The bending of curve towards real Z' axis shows a tendency of formation of a semicircular arc. The bulk resistance (R_g) of the composite increases compared to PVDF and BFO-BST nano-ceramics. The value of grain and grain boundary contribution to the total resistance of the nanocomposite are compared in Table 1. It can be clearly noticed that the value of R_g decreases with rise in temperature for all samples with a clear indication of NTCR behavior of the sample. It is evident from Nyquist plots; that multiple relaxation times and processes are associated with grain and grain boundaries. The multiple broad dielectric relaxations is interrelated to various factors including size-distribution, wall-motion and orientation of domains, defect dipoles created causing diffuse dielectric transition.

Fig. 5 Nyquist plot of (1 - x)PVDF-x(BFO-BST) (x = 0.05,0.10,0.15)

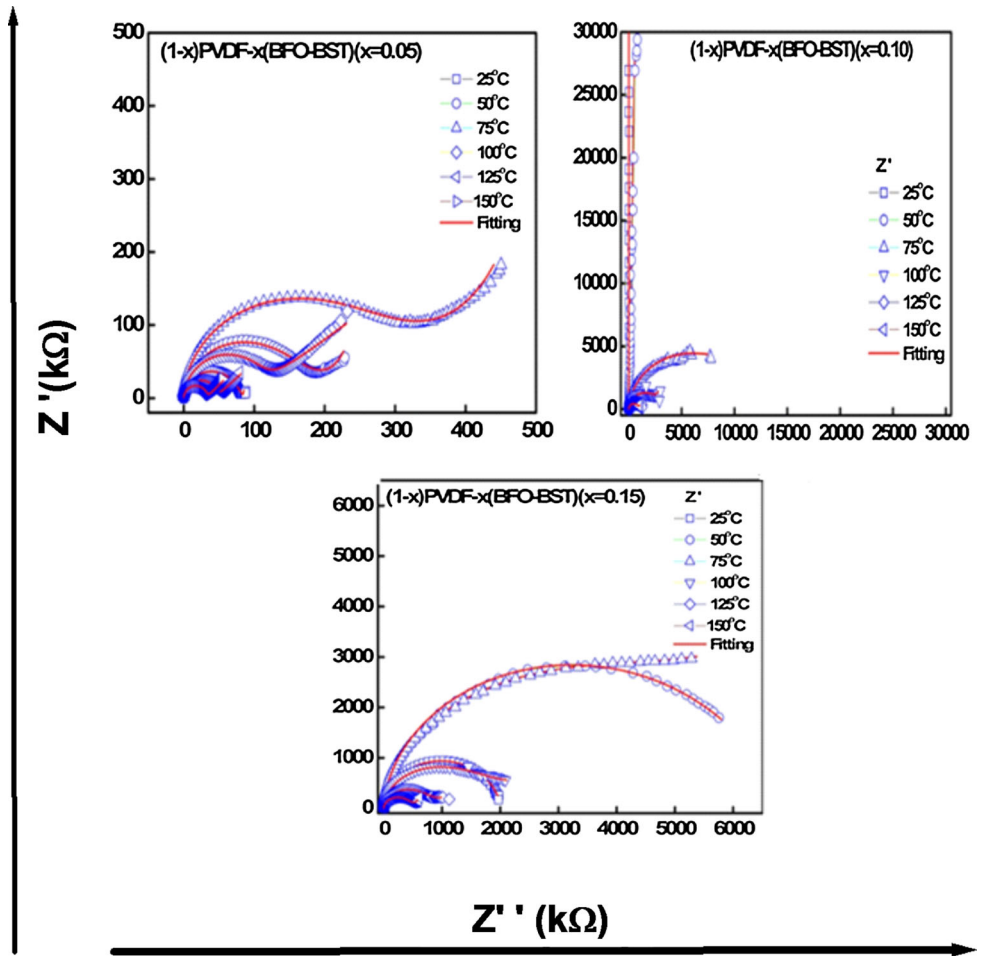


Table 1 Comparison of resistance and capacitance of grain (R_g and C_g) and grain boundary (R_{gb} and C_{gb}) contribution to the total resistance and capacitance of (1 - x)PVDF-x(BFO-BST) (x = 0.05,0.10 and 0.15) nanocomposite

Composite name	Temp. (°C)	R_g (Ω)	C_g (F)	R_{gb} (Ω)	CPE	C_{gb} (F)
(1 - x)PVDF-x(BFO-BST) (x = 0.05)	25	4.737E4	3.486E-7	8.720E4	3.470E-8	1.058E-10
	50	5.295E4	8.784E-8	5.662E5	1.296E-7	1.067E-10
	75	3.477E3	3.467E-8	1.000E7	1.111E-6	1.044E-10
	100	9.551E3	3.365E-10	7.336E8	5.833E-8	1.425E-10
	125	4.510E4	5.004E-10	1.000E8	1.387E-8	1.214E-10
	150	3.196E4	3.312E-6	1.000E8	1.707E-6	1.252E-10
(1 - x)PVDF-x(BFO-BST) (x = 0.10)	25	1.000E7	1.569E-10	-	1.216E-10	-
	50	1.000E2	1.023E-10	-	1.023E-10	-
	75	1.435E2	9.474E-10	2.258E7	1.175E-8	9.946E-11
	100	1.742E5	3.906E-10	3.824E8	1.878E-8	1.032E-10
	125	2.526E3	2.382E-8	2.733E8	4.592E-7	1.027E-10
	150	2.480E1	1.766E-8	1.468E6	9.773E-10	1.042E-10
(1 - x)PVDF-x(BFO-BST) (x = 0.15)	25	1.000E7	3.470E-8	1.987E6	1.409E-10	9.418E-11
	50	2.122E1	7.240E-9	1.000E8	5.957E-8	9.986E-11
	75	1.000E7	1.193E-5	7.013E6	1.007E-9	9.631E-11
	100	1.866E6	8.948E-10	1.000E8	2.235E-7	1.000E-10
	125	2.216E1	8.052E-11	5.751E8	5.803E-7	1.009E-10
	150	2.762E0	4.063E-8	6.386E8	1.070E-6	1.034E-10

3.4 Electrical modulus study

The Fig. 6 show the variation of real part of dielectric modulus (M') and imaginary part (M'') as a function of frequency over a range of temperature for all three composite of $(1-x)\text{PVDF}-x(\text{BFO}-\text{BST})$ ($x = 0.05, 0.1, 0.15$). At low frequencies and temperatures, M' tends to be very small but not approaching zero. This indicates that electrode polarization makes a significant contribution at lower temperature and space charge accumulates at the interface. Moreover, a continuous increase in the value of M' has been observed with increasing frequency, with a tendency to level off at higher frequencies, in the usual sigmoidal manner, for all the temperatures and all composites. This observation may possibly be related to a lack of restoring force governing the mobility of charge carriers under the action of an induced electric field [22]. As increase in the value of M' with increasing frequency may be attributed to the relaxation phenomena, because of the short range mobility of the charge carrier, which is spread over a range of frequency.

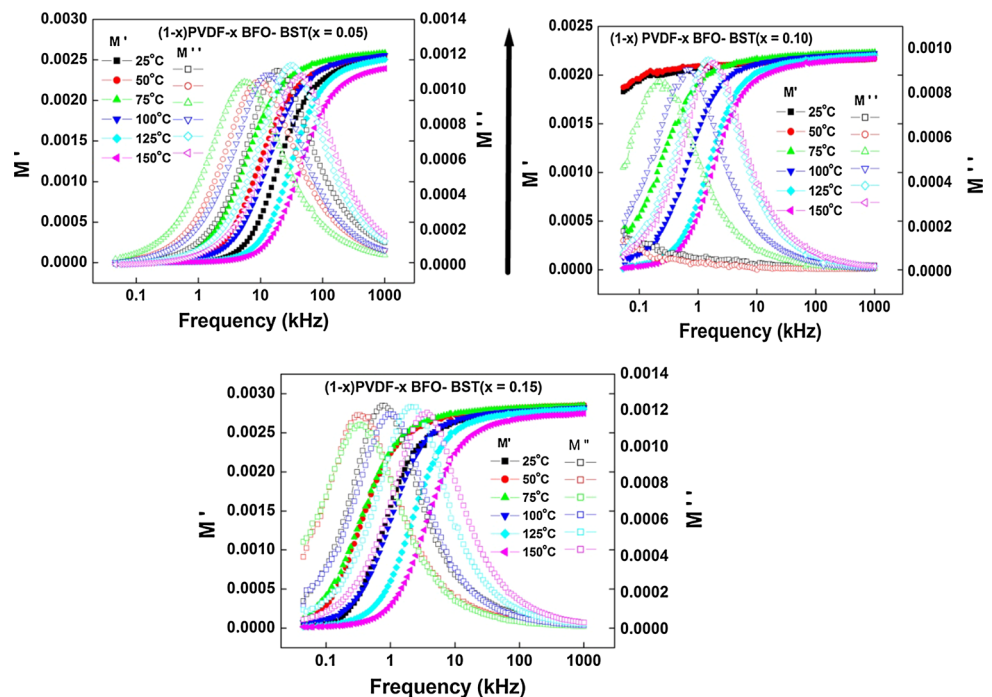
Figure 6 also compares the variation of the imaginary part of the dielectric modulus (M'') as a function of frequency at different temperature of $(1-x)\text{PVDF}-x(\text{BFO}-\text{BST})$ ($x = 0.05, 0.1, 0.15$). The variation of M'' with frequency at different temperature gives useful information about the mechanism of charge transport, for the example electrical transport and conductivity relaxation. In all temperature range for the entire composite the modulus plot are characterized by well defined asymmetric peaks at different frequencies. For all the samples, the plots obtained in each temperature; asymmetric relative to the

peak maxima and the peak are much broader than that would be predicted by ideal Debye behavior. The broader nature of the peaks can be interpreted as the consequence of the distribution of relaxation time because of non-Debye type relaxation behavior of the material. In the low frequency region (to the left side of the peak) the charge carriers can be regarded as mobile over long distances and as performing successful hopping from one site to another. At higher frequencies (to the right side of the peaks), however the charge carrier motion is confined and only localized movement is observed. The frequency region in which the peak occurs is indicative of the transition from long-range to short range mobility of the ions [23]. Moreover, the maximum of the peak frequency shifts towards higher frequencies with increasing temperature as well as BFO–BST wt% or concentration. The shifting of the peak suggests that the relaxation in which the hopping of charge carriers may occur is thermally activated. This behavior also suggests that the relaxation time decreases with increasing temperature as well as wt% of the BFO–BST concentration.

3.5 Electric and magnetic hysteresis study

Figure 7 Shows the P–E hysteresis loop of pure PVDF and $(1-x)\text{PVDF}-x(\text{Bi}_{0.5}\text{Ba}_{0.25}\text{Sr}_{0.25})(\text{Fe}_{0.5}\text{Ti}_{0.5})\text{O}_3$ ($x = 0.05, 0.1, 0.15$) nanocomposite at 50 Hz at room temperature. In order to have a clear idea regarding the polarization behavior; all the composites were pooled at an applied unique field i.e., about 60 kV/cm. There is the

Fig. 6 Frequency dependent M' and M'' spectrum of $(1-x)\text{PVDF}-x(\text{BFO}-\text{BST})$ ($x = 0.05, 0.10$ and 0.15)



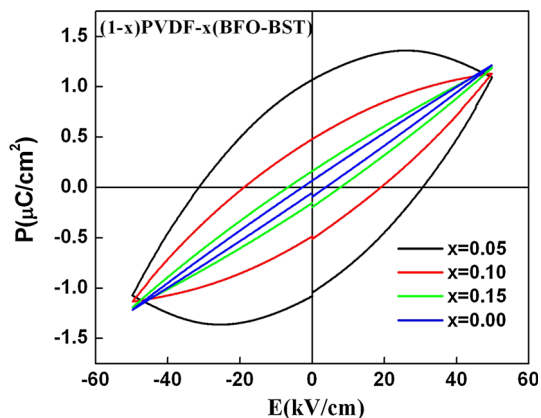


Fig. 7 Hysteresis loop of pure PVDF and (1 - x)PVDF-x(BFO-BST) (x = 0.05, 0.10 and 0.15) nanocomposite

formation of a well defined non-linear, unsaturated loop for PVDF. The value of saturation polarization for the case of pure PVDF is found to be $>1 \mu\text{C}/\text{cm}^2$ and for all other composite it is also found that the saturation polarization in the same range. Small values of saturation polarization of PVDF have been consistent with the earlier reported one [24]. The observed well defined ferroelectric hysteresis loops for (x = 0.05) demonstrate that the nanocomposite film retains good ferroelectric properties. The remnant polarization for (x = 0.05) is more than that of x = 0.10 and x = 0.15 and the saturation polarization is almost same for all three nanocomposite. The appearance of lossy loop for x = 0.05 suggests that the composite may not be suitable for capacitive energy storage device as the area under the loop is quite more than that of x = 0.10 and x = 0.15 of composite. Whereas the slim loop of x = 0.10 and x = 0.15 are quite encouraging for the application of the composite in capacitive energy storage device. In the other hand it is found that the x = 0.05 composite is suitable candidate for memory device application. The slim loop of x = 0.15, nanocomposite is equivalent shape to that of the virgin PVDF. The possible reason for the appearance of proper ferroelectric loop in case x = 0.05 composite can be attributed to the critical filler load beyond which it cannot commensurate with the field. This suggests that there is a critical point for the filler BFO-BST concentration and which suggests that the long-range ordered dipole chains of the copolymer phase are not destroyed as long as the BFO-BST particle fraction is below the critical point. Beyond this critical point, however the remnant polarization decreases. That is why it becomes virtually impossible to obtain saturated hysteresis loop at the measured frequency. The value of saturation polarization of the synthesized nanocomposite is quite less than the pure PVDF. From Fig. 8 it is found that the M-H loop of the x = 0.15 is not encouraging because PVDF matrix is itself a non magnetic polymer which causes the reduction in

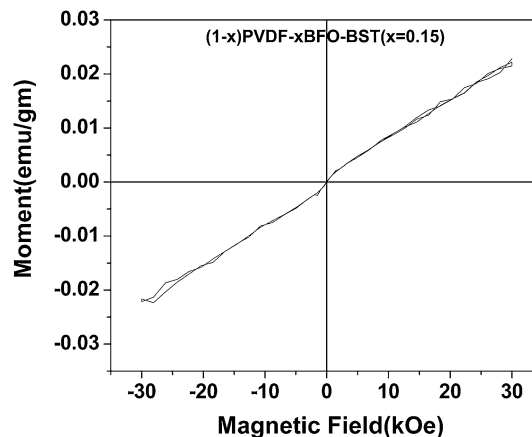


Fig. 8 H-H loop of (1 - x)PVDF-x(BFO-BST) (x = 0.15)

magnetization. The possible reason of the decrease in magnetization may be as follows: firstly, the non magnetic PVDF polymer coating layer, can be envisaged as a magnetic dead layer on the ceramic, thus affecting the magnitude of magnetization due to the quenching of the surface moment [25]. Secondly, the magnetization of the composite is related to the volume fraction of the ferrite particle by the relation $M_s = \phi m_s$, where ϕ the volume fraction of the ferrite particle and m_s is the saturation moment of a single particle [26]. On increasing non-magnetic PVDF concentration in the composite films, the BFO-BST ferrite phase volume fraction in composite decreases thereby decreasing the total magnetization.

3.6 ME measurement

Magneto-electric effect, a coupled ferroelectric and magnetic effect refers to the electric field inspired magnetization and magnetic field induced electric polarization. The coupling of ME effect is generally characterized by ME voltage coefficient α_E which can be defined as [27, 28].

$$\text{The ME coefficient} = \frac{dE}{dH} = \frac{1}{d} \frac{dV}{dH} = \frac{V_{out}}{h_o d}$$

where E is the induced electric field, H is the applied magnetic field, V is the ME voltage developed across the sample, h_o is the magnitude of the AC magnetic field and d is thickness of the sample. ME coefficient has been measured by dynamic method involving simultaneous application of AC as well as DC magnetic field [29]. The voltage developed across the (1 - x)PVDF-xBFO-BST (x = 0.05,0.10,0.15) samples were measured using a ME set up with lock-in-amplifier. In our experiment, 15.37 Oe AC magnetic fields and 1 kHz frequency were applied along with a DC magnetic field of varying magnitude (-5 to +5 kOe). The variation of ME voltage coefficient with applied DC magnetic field of (1 - x)PVDF-

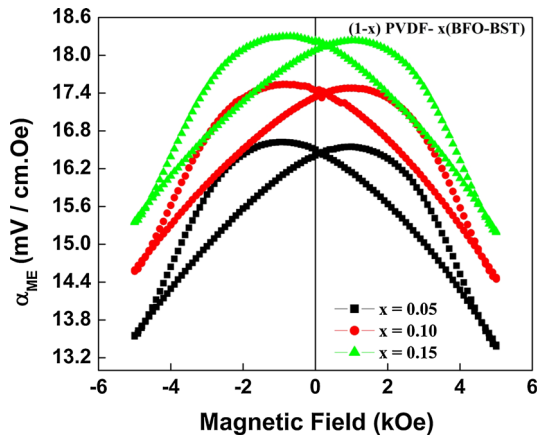


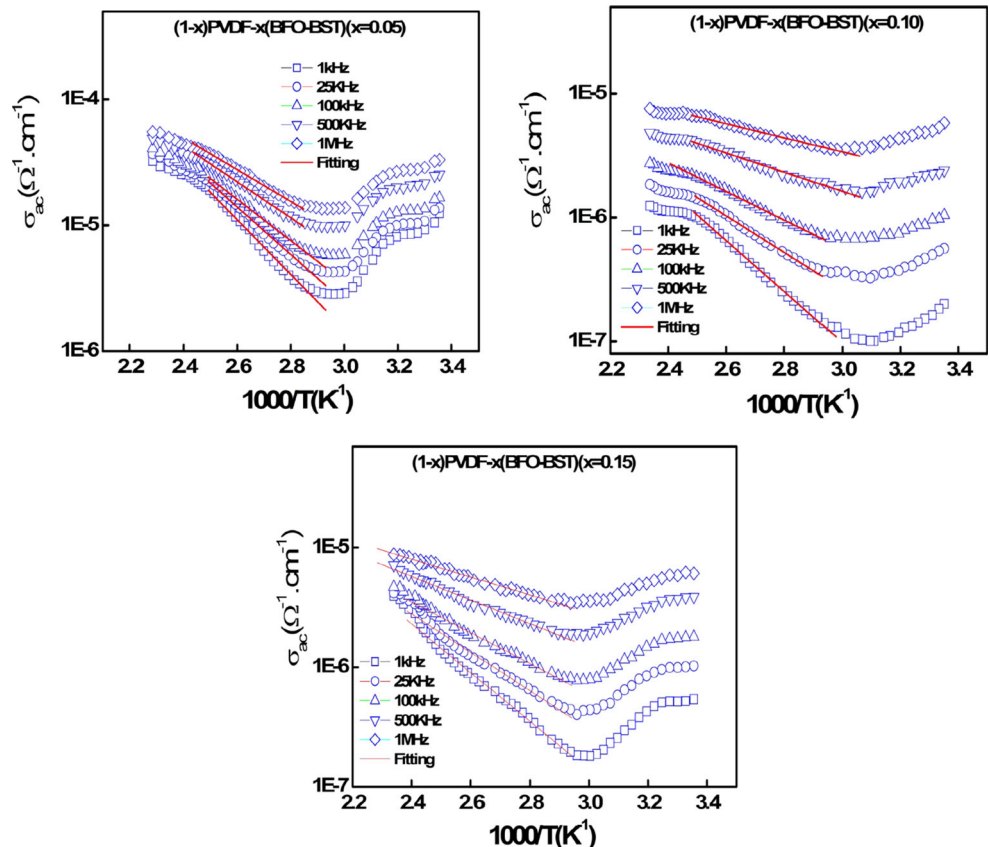
Fig. 9 M–E loop of (1 - x)PVDF-x(BFO-BST) (x = 0.05, 0.10 and 0.15)

$x(\text{Bi}_{0.5}\text{Ba}_{0.25}\text{Sr}_{0.25})(\text{Fe}_{0.5}\text{Ti}_{0.5})\text{O}_3$ (x = 0.05, 0.10 and 0.15) sample is shown in Fig. 9. As reported earlier [30], the ME voltage developed across the sample due to the application of magnetic field can be written as:

$$E = V/d = f(H) = \text{constant} + \alpha H + \beta H^2 + \gamma H^3 + \delta H^4 + \tag{1}$$

$$\Rightarrow \frac{dE}{dH} = \alpha + 2\beta H + 3\gamma H^2 + 4\delta H^3 + \tag{2}$$

Fig. 10 Temperature dependent AC conductivity of (1 - x) PVDF-x(BFO-BST) (x = 0.05, 0.10 and 0.15) nanocomposite



The AC field (h) superimposed into the DC field (H) can be written as; $h = h_0 \sin \omega t$ and the total magnetic field can be expressed as:

$$H_{total} = H + h_0 \sin \omega t \tag{3}$$

The magnitude of the AC field (h_0) can be calculated from the following expression.

$$h_0 = 0.899 \times \frac{NI}{R} \tag{4}$$

where N is the number of turns of the Helmholtz coil, I is the current in Ampere and R is radius of the coil in cm. From the above equation the value of found to be 15.37 gauss. At zero magnetic field the ME voltage coefficient (α_{ME}) was found to be 16.4, 17.6 and 18.4 mV/cm. Oe for (1 - x)PVDF-x(Bi_{0.5}Ba_{0.25}Sr_{0.25})(Fe_{0.5}Ti_{0.5})O₃ (x = 0.05, 0.1 and 0.15). The lowest value of ME coefficient for x = 0.05 can be attributed to the lower value of filler concentration in the PVDF matrix. This result can be correlated with the consistent results that were obtained from dielectric, magnetic and polarization study.

3.7 AC conductivity

The activation energy E_a , based on a thermally activated process, can be calculated using the relation:

$$\sigma_{ac} = \sigma_0 \exp(-E_a/kT) \tag{5}$$

where k = Boltzmann constant and σ_0 = pre-exponential factor. The temperature dependence of ac conductivity of different polymer nano-composite at different frequencies is shown in Fig. 10. The Arrhenius plot ($\log \sigma_{ac}$ vs. $1000/T$) in which the value of $\log \sigma_{ac}$ increases linearly with the increase in temperature. The estimated (using linear fitting) value of activation energy can be calculated from different region of the plot. For each frequency in the plots, occurrence of different slopes in the different temperature regions suggests the presence of multiple conduction processes in these samples with different activation energy. Study of frequency dependence of electrical conductivity provides the vital information on dominant constituents or charge species involved in the conduction process. Such study was carried out for our samples using double Jonscher’s power law.

The increasing nature of conductivity with temperature can be well understood by the help of free-volume model [31]. With increases in temperature, the polymer can expand easily and it is easy to produce free volume. As, a result with increase in temperature, the free volume increases. The resulting conductivity, represented by the overall mobility of ions and the polymer, is determined by the free volume around the polymer chains. Hence, as temperature increases, ions, solvated molecules, or polymer segments can move into the free volume. This leads to an increase in ion mobility and segmental mobility that will assist ion transport and virtually compensate for the retarding effect of the ion clouds [32, 33].

Table 2 Activation energy calculated from temperature dependent ac conductivity

Composite name	Frequency	E_a (eV)
(1 - x)PVDF-x(BFO-BST) (x = 0.05)	1 kHz	0.431
	25 kHz	0.374
	100 kHz	0.325
	500 kHz	0.283
	1 MHz	0.250
(1 - x)PVDF-x(BFO-BST) (x = 0.05)	1 kHz	0.407
	25 kHz	0.292
	100 kHz	0.228
	500 kHz	0.153
	1 MHz	0.112
(1 - x)PVDF-x(BFO-BST) (x = 0.05)	1 kHz	0.405
	25 kHz	0.319
	100 kHz	0.256
	500 kHz	0.196
	1 MHz	0.149

The observed increase in ionic conductivity with the increase of temperature is ascribed to the decrease in viscosity and hence to the increased chain flexibility [34]. The segmental motion either allows the ions to hop from one site to another or provide an alternative for ions to move. Thus the segmental motion of (1 - x)PVDF-x(BFO-BST) facilitate the translational motion [34]. The activation energy calculated in the high temperature range using the above Eq. (5) is presented in Table 2. From the table it is clear that the change in activation energy with increase in filler concentration. Over all from the activation energy it is evident that the predominant electron conduction mechanism is playing in the composite because of low value of activation energy. Beside this in $x = 0.05$ composite somehow show a mixed conduction mechanism (electron as well as polaron hopping) is found because of little high value of activation energy (more thn 0.4 eV at 25 kHz in all three composite). From activation energy it is also clear that with increase in frequency the activation energy decreases.

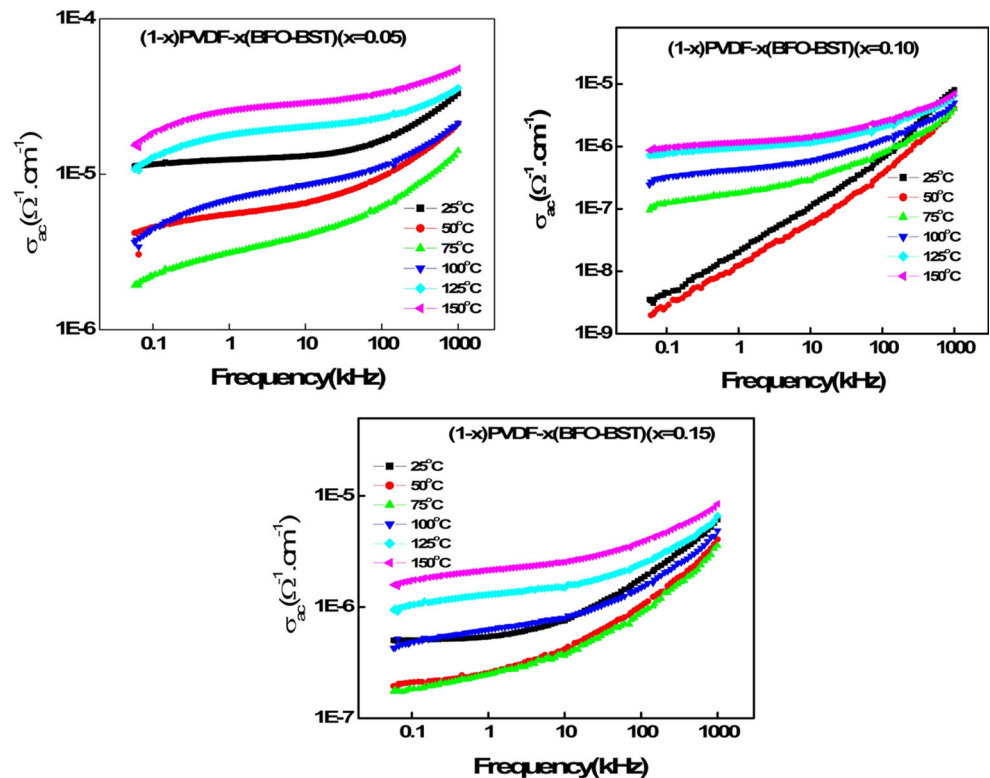
Figure 11 shows the variation of σ_{ac} with frequency at selected temperatures from 25 to 125 °C with a difference of 25 °C (1, 25, 100, 500 kHz and 1 MHz) of (1 - x)PVDF-x(BFO-BST) ($x = 0.05, 0.10$ and 0.15). It is observed from both figures that the frequency dependence of conductivity spectra shows two regimes, (a) the low-frequency plateau region and (b) the high-frequency dispersion region. The low-frequency plateau region corresponds to the frequency-independent conductivity σ_o (or) σ_{dc} .

All the data were well agreement with Jonscher power law: $\sigma_{ac} = \sigma_{dc} + A\omega^n$ ($0.1 \leq n \leq 1.0$) where σ_{dc} = dc-conductivity and A is temperature dependent factor. Generally, ac conductivity increases on increasing frequency and temperature in polycrystalline materials. It is observed that ac conductivity is almost frequency independent at lower frequencies, forming a plateau region [15, 16]. The frequency independent conductivity is considered as dc conductivity of the materials, which can be due to thermally assisted space charge carriers. Hence, it can be concluded that further increase of ceramics filler concentration in the PVDF matrix can further reduce the electrical properties, and hence materials may not be useful for meaningful devices.

4 Summary and conclusion

Pure PVDF and (1 - x)PVDF-x(Bi_{0.5}Ba_{0.25}Sr_{0.25})(Fe_{0.5}Ti_{0.5})O₃ ($x = 0.05, 0.1$ and 0.15) nano-composites were prepared by a solution casting method using NMP as solvent. Structural analysis confirms the co-existence of α and γ -phase in pure PVDF polymer. In all the composition of ceramic-polymer nano-composite both the phase has

Fig. 11 Frequency dependent ac conductivity of $(1-x)$ PVDF- x (BFO-BST) ($x = 0.05, 0.10$ and 0.15) nanocomposite



equally a priority depending on their percentage value. The HRTEM micrograph of the prepared ceramic is found to be in nano-regime with less agglomeration. Study of SEM micrograph shows excellent distribution of BFO-BST nano ceramic in the PVDF matrix without. The enhanced dielectric constant of the PVDF based polymer nano composite could be suitable for energy storage devices. Nyquist plot shows a tendency of differencing grain and grain boundary effect in the polymer nano-composite. All the extracted properties of the multiferroic polymer nanocomposites suggest that this composite can be a promising candidate for room temperature multiferroic devices.

Acknowledgments The authors gratefully acknowledge the grant received from DRDO (Grant Number: ERIP/ER/1102202/M/01/1438 dated 25/07/2012) Government of India to carry out this work. The authors also grateful to CRF, IIT Kharagpur and Dr. Ashok Kumar, Senior Scientist of NPL, New Delhi, for providing some experimental facilities.

References

1. A.J. Lovinger, Ferroelectric polymers. *Science* **220**, 115 (1983)
2. H. Kawai, The piezoelectricity of poly(vinylidene fluoride). *Jpn. J. Appl. Phys.* **8**, 975 (1969)
3. M. Kobayashi, K. Tashiro, H. Tadokoro, Molecular vibrations of three crystal forms of poly(vinylidene fluoride). *Macromolecules* **8**, 158 (1975)
4. A. Bello, E. Laredo, M. Grimau, Distribution of relaxation times from dielectric spectroscopy using Monte Carlo simulated annealing: application to α -PVDF. *Phys. Rev. B* **60**, 12764 (1999)
5. K. Kakimoto, K. Fukuta, H. Ogawa, Fabrication of fibrous BaTiO₃-reinforced PVDF composite sheets for transducer application. *Sens. Actuators, A* **200**, 21 (2013)
6. T. Zhou, J.W. Zha, R.Y. Cui, B.H. Fan, J.K. Yuan, Z.M. Dang, Improving dielectric properties of BaTiO₃/ferroelectric polymer composites by employing surface hydroxylated BaTiO₃ nanoparticles. *ACS Appl. Mater. Interfaces* **3**, 2184 (2011)
7. W.M. Xia, Z. Xu, F. Wen, Z.C. Zhang, Electrical energy density and dielectric properties of poly(vinylidene fluoride-chlorotrifluoroethylene)/BaSrTiO₃ nanocomposite. *Ceram. Int.* **38**, 1071 (2012)
8. H. Hammami, M. Arous, M. Lagache, A. Kallel, Study of the interfacial MWS relaxation by dielectric spectroscopy in unidirectional PZT fibres/epoxy resin composites. *J. Alloys Compd.* **430**, 1 (2007)
9. C. Behera, R.N.P. Choudhary, P.R. Das, Structural, dielectric, impedance and magneto-electric properties of mechanically synthesized(Bi_{0.5}Ba_{0.25}Sr_{0.25})(Fe_{0.5}Ti_{0.5})O₃ nano-electronic system. *Mater. Res. Express* **3**, 035005 (2016)
10. H. Khelifi, M. Zannen, N. Abdelmoula, D. Mezzane, A. Maalej, H. Khemakhem, M. Es-Souni, Dielectric and magnetic properties of $(1-x)$ BiFeO₃- x Ba_{0.8}Sr_{0.2}TiO₃ ceramics. *Ceram. Int.* **38**, 5993 (2012)
11. S. Liu, S. Xue, W. Zhang, J. Zhai, G. Chen, Significantly enhanced dielectric property in PVDF nano-composites flexible films through a small loading of surface-hydroxylated Ba_{0.6}Sr_{0.4}TiO₃ nanotubes. *J. Mater. Chem. A* **2**, 18040 (2014)
12. A. Tawansi, A.H. Oraby, H.I. Abdelkadar, M. Abdelaziz, FeCl₃-CoCl₂ mixed fillers effects on the structural, electrical and magnetic properties of PVDF films. *J. Magn. Mater.* **262**, 203 (2003)
13. I.S. Elashmawi, E.M. Abdelrazek, H.M. Ragab, N.A. Hakeem, Structural, optical and dielectric behaviour of PVDF filled with

- different concentration of iodine PVDF-PZT nanocomposite film based self-charging power cell. *Phys. B* **405**, 94 (2010)
14. S. Sen, S.K. Mishra, Electrical behavior of PMN-PT-PVDF nanocomposite. *J. Phys. D Appl. Phys.* **41**, 165305 (2008)
 15. Y. Zhang, Y. Zhang, X. Xue, C. Cui, B. He, Y. Nie, P. Deng, Z.L. Wang, Structural, electrical and dielectric properties of $(\text{Sr}1 - x\text{CaX})\text{MnO}_3$ ($0 \leq x \leq 1.0$) ceramic. *Nanotechnology* **25**, 105401 (2014)
 16. S. Dash, R.N.P. Choudhary, M.N. Goswami, Modification of ferroelectric and resistive properties of $(\text{Bi}_{0.5}\text{Na}_{0.5})(\text{Nb}_{0.5}\text{Fe}_{0.5})\text{O}_3$ -PVDF composite. *J. Polym. Res.* **22**, 54 (2015)
 17. P. Mishra, P. Kumar, Dielectric properties of 0.25(BZT-BCT) - 0.75[(1 - x)PVDF-xCCTO] ($x = 0.02, 0.04, 0.06, 0.08$ and 0.1) composites for embedded capacitor application. *Compos. Sci. Technol.* **88**, 26 (2013)
 18. L.L. Sun, B. Li, Y. Zhao, G. Mitchell, W.H. Zhong, Structure-induced high dielectric constant and low loss of CNF/PVDF composites with heterogeneous CNF distribution. *Nanotechnology* **21**, 305702 (2010)
 19. A.K. Zak, W.C. Gan, W.A. Majid, M. Darroudi, Experimental and theoretical dielectric studies of PVDF/PZT nanocomposite thin films. *Ceram. Int.* **37**, 1653 (2011)
 20. F.C. Loh, K.L. Tan, E.T. Kang, Y. Uyama, Y. Ikada, Structural studies of polyethylene, poly(ethylene terephthalate) and polystyrene films modified by near u.v. light induced surface graft copolymerization. *Polymer* **36**, 21 (1995)
 21. Y. Deng, Y. Zhang, Y. Xiang, G. Wang, X. Huibin, Bi_2S_3 - BaTiO_3 /PVDF three-phase composites with high dielectric permittivity. *J. Mater. Chem.* **19**, 2058 (2009)
 22. M. Pant, D.K. Kanchan, N. Gondaliyam, Transport properties and relaxation studies in BaO substituted $\text{Ag}_2\text{O}-\text{V}_2\text{O}_5-\text{TeO}_2$ glass system. *Mater. Chem. Phys.* **115**, 98 (2009)
 23. J. Liu, C.G. Duan, W.G. Yin, W.N. Mei, R.W. Smith, J.R. Hardy, Dielectric permittivity and electric modulus in $\text{Bi}_2\text{Ti}_4\text{O}_{11}$. *J. Chem. Phys.* **119**, 2812 (2003)
 24. S. Satpathy, P.K. Gupta, K.B.R. Verma, Enhancement of non-volatile polarization and pyroelectric sensitivity in lithium tantalite(LT)/poly(vinylidene fluoride) (PVDF) nanocomposite. *J. Phys. D Appl. Phys.* **42**, 055402 (2009)
 25. R. kaiser, G. Miskolczy, Magnetic properties of stable dispersion of subdomain magnetic particle. *J. Appl. Phys.* **41**, 1064 (1970)
 26. G.D. Prasanna, H.S. Jayanna, A.R. Lamanian, S. Dash, Polyaniline/CoFe₂O₄ nanocomposite: a novel synthesis, characterization and magnetic properties. *Synth. Met.* **161**, 2306 (2011)
 27. Y. Zhanga, J.P. Zhou, Q. Liu, S. Zhang, C.Y. Deng, Dielectric, magnetic and magnetoelectric properties of Ni_{0.5}Zn_{0.5}Fe₂O₄-Pb(Zr_{0.48}Ti_{0.52})O₃ composite ceramics. *Ceram. Int.* **40**, 5853 (2014)
 28. M. Shi, R. Zuo, Y. Xun, L. Wang, C. Gu, H. Su, J. Zhong, G Yu Preparation and multiferroic properties of 2-2 type CoFe₂O₄/Pb(Zr, Ti)O₃ composite films with different structures. *Ceram. Int.* **40**, 9249 (2014)
 29. G.V. Duonga, R. Groessinger, M. Schoenhardt, D. Bueno-Basques, The lock-in technique for studying magnetoelectric effect. *J. Magn. Magn. Mater.* **316**, 390s (2007)
 30. J. Miao, H. Yang, W. Hao, J. Yuan, B. Xu, X.Q. Qiu, L.X. Cao, B.R. Zhao, Temperature dependence of the ferroelectric and dielectric properties of the $\text{B}_{0.5}\text{Sr}_{0.5}\text{TiO}_3/\text{La}_{0.67}\text{Sr}_{0.33}\text{MnO}_3$ Heterostructure. *J. Phys. D Appl. Phys.* **38**, 5 (2005)
 31. S. Rajendran, T. Uma, Lithium ion conduction in PVC-LiBF₄ electrolytes gelled with PMMA. *J. Power Sources* **88**, 282 (2000)
 32. D. Saikia, Y.W. Chen-Yang, Y.T. Chen, Y.K. Li, S.I. Lin, Investigation of ionic conductivity of composite gel polymer electrolyte membranes based on P(VDF-HFP), LiClO₄ and silica aerogel for lithium ion battery. *Desalination* **234**, 24 (2008)
 33. K. Tsunemi, H. Ohno, E.A. Tsuchida, Mechanism of ionic conduction of poly (vinylidene fluoride)-lithium perchlorate hybrid films. *Electrochim. Acta* **28**, 833 (1983)
 34. S. Ramesh, O.P. Ling, Effect of ethylene carbonate on the ionic conduction in poly(vinylidene fluoride-hexafluoropropylene) based solid polymer electrolytes. *Polym. Chem.* **1**, 702 (2010)